Magnetic Ordering and Spin-Glass Behavior in First-Row Transition Metal Hexacyanomanganate(IV) Prussian Blue Analogues

Wayne E. Buschmann and Joel S. Miller*

Department of Chemistry, University of Utah, 315 S. 1400 E. Rm 2124, Salt Lake City, Utah 84112-0850

Received November 9, 1999

Magnetically ordered Prussian blue analogues with the general formulation of $M[Mn(CN)_6]$ (M = V, Cr, Mn, Co, Ni) were made in aprotic media utilizing $[Mn^{IV}(CN)_6]^{2-}$. These analogs are valence-ambiguous, as they can be formulated as $M^{II}[Mn^{IV}(CN)_6]$ or $M^{III}[Mn^{III}(CN)_6]$. The X-ray powder diffraction of each member of this family can be indexed to the face-centered cubic (fcc) Prussian blue structure type, with atypically reduced unit cell parameters ($a \approx 9.25 \pm 0.25$ Å) with respect to hydrated Prussian blue structured materials ($a \geq 10.1$ Å). The reduced *a*-values are attributed to a contraction of the lattice in the absence of water or coordinating solvent molecule (i.e., MeCN) that is necessary to help stabilize the structure during lattice formation. Based on ν_{CN} IR absorptions, X-ray photoelectron spectra, and magnetic data, the following oxidation state assignments are made: $M^{II}[Mn^{IV}(CN)_6]$ (M = Co, Ni) and $M^{III}[Mn^{III}(CN)_6]$ (M = V, Cr, Mn). Formation of $Mn^{III}[Mn^{III}(CN)_6]$ is in contrast to $Mn^{II}[Mn^{IV}(CN)_6]$ prepared from aqueous media. Above 250 K, the magnetic susceptibilities of $M[Mn(CN)_6]$ (M = V, Cr, Mn, Co, Ni) can be fit to the Curie−Weiss equation with $\theta = -370$, -140, -105, -55, and -120 K, respectively, suggesting strong antiferromagnetic coupling. The room temperature effective moments, respectively, are 3.71, 4.62, 5.66, 4.54, and 4.91 μ_B, consistent with the above oxidation state assignments. All compounds do not exhibit magnetic saturation at 50 kOe, and exhibit frequency-dependent $\chi'(T)$ and $\chi''(T)$ responses characteristic of spin-glass-like behavior. $M[Mn(CN)_6]$ order as ferrimagnets, with T_c's taken from the peak in the 10 Hz $\chi'(T)$ data, of 19, 16, 27.1, <1.75, and 4.8 K for M = V, Cr, Mn, Co, and Ni, respectively. The structural and magnetic disorder prevents $Ni^{II}[Mn^{IV}(CN)_6]$ from ordering as a ferromagnet as anticipated, and structural inhomogeneities allow $Co^{II}[Mn^{IV}(CN)_6]$ and $V^{III}[Mn^{III}(CN)_6]$ to unexpectedly order as ferrimagnets. Also, $Mn^{III}[Mn^{III}(CN)_6]$ behaves as a reentrant spin glass showing two transitions at 20 and 27.1 K, and similar behavior is evident for $Cr^{III}[Mn^{III}(CN)_6]$. Hysteresis with coercive fields of 340, 130, 8, 9, and 220 Oe and remanent magnetizations of 40, 80, 1500, 4, and 250 emuOe/mol are observed for M = V, Cr, Mn, Co, and Ni, respectively.

Introduction

The face-centered cubic (fcc) Prussian blue structure type with →M←C≡N→M′←N≡C→M← linkages along all three directions and relative ease to vary the metal ion, charge, and consequently number of spins per site, can lead to a variety of magnetic behavior. Ferromagnetic coupling, which may lead to ferromagnetic ordering, can be achieved when spins on adjacent metal ion sites are in orthogonal orbitals in accord with Hund's rule.[1−3] The octahedral coordination by cyanide ligands bridges between the metals, one low-spin *C*-bound (M) and the other high-spin *N*-bound (M′). This behavior is exemplified by Prussian blue, $Fe^{III}_4[Fe^{II}(CN)_6]_3$, **1**; however, because of the high-spin Fe^{III}/low-spin Fe^{II}/1/0.75 ratio, each unit cell lacks one low-spin Fe^{II} ion, and consequently the structure is defect-rich (accommodating 14 H_2O's) and lacks the maximal number of nearest-neighbor interactions necessary for strong magnetic coupling.[4a] Nonetheless, **1**, which furthermore has weak magnetic coupling as it possesses spinless ($S = 0$) Fe^{II}, orders ferromagnetically at 5.6 K.[4b]

Hence, when the spin-containing orbitals are of the same symmetry (i.e., both sites contain spins in the t_{2g} or e_g orbitals), the unpaired electron spins couple antiferromagnetically. When the antiferromagnetic spins compensate each other, antiferromagnetic ordering can occur. However, if they do not compensate, a net moment will occur that can lead to ferrimagnetic ordering. In contrast, when the neighboring spin-containing orbitals are orthogonal to one another (i.e., spins in the t_{2g} orbitals neighboring spins in the e_g orbitals), the unpaired electrons will couple ferromagnetically, in accord with Hund's rule.[2a] To achieve ferromagnetic coupling in this manner, which can lead to ferromagnetic ordering, appropriate combinations of metal ions are essential. This requires neighboring d^8 (e_g^2) and d^3 (t_{2g}^3) metal ions as in $CsNi^{II}[Cr^{III}(CN)_6]\cdot 2H_2O$, which orders ferromagnetically below its critical temperature, T_c, of 90 K.[3] Several other examples are also reported using this strategy with short-range ferromagnetic coupling leading to bulk

* Author to whom all correspondence should be addressed.

(1) (a) Mallah, T.; Ferlay, S.; Auberger, C.; Hélary, C.; L'Hermite, F.; Ouahés, R.; Vaissermann, J.; Verdaguer, M.; Veillet, P. *Mol. Cryst. Liq. Cryst.* **1995**, *273*, 141. (b) Entley, W. R.; Treadway, C. R.; Girolami, G. S. *Mol. Cryst. Liq. Cryst.* **1995**, *273*, 153. (c) Gadet, V.; Bujoli-Doeuff, M.; Force, L.; Verdaguer, M.; Malkhi, K. E.; Deroy, A.; Besse, J. P.; Chappert, C.; Veillet, P.; Renard, J. P.; Beauvillain, P. In *Magnetic Molecular Materials*; Gatteschi, D., Kahn, O., Miller, J. S., Palacio, F., Eds.; NATO Advanced Study Institute Series E; Plenum: New York, 1991; Vol. 198, pp 281−295.

(2) (a) Miller, J. S. Epstein, A. J., *Angew. Chem.* **1994**, *33*, 385. Miller, J. S.; Epstein, A. J. *Chem. Eng. News* **1995**, *73* #40, 30. (b) Kahn, O. *Molecular Magnetism*; VCH Publishers: New York, 1993.

(3) Gadet, V.; Mallah, T.; Castro, I.; Verdaguer, M.; Veillet, P. *J. Am. Chem. Soc.* **1992**, *114*, 9213.

(4) (a) Buser, H. J.; Schwarzenbach, D.; Petter, W.; Ludi, A. *Inorg. Chem.* **1977**, *16*, 2704. (b) Herren, F.; Fischer, P.; Ludi, A.; Hälg, W. *Inorg. Chem.* **1980**, *19*, 956.

10.1021/ic991308y CCC: $19.00
Published on Web 05/10/2000

Table 1. Examples of Ferromagnetically Ordered Prussian Blue Structured Compounds

compound	a (Å)[a]	θ (K)	T_c (K)	reference
$CsNi^{II}[Cr^{III}(CN)_6]\cdot 2H_2O$	10.57	[b]	90	3
$Ni^{II}_3[Cr^{III}(CN)_6]_2\cdot 9H_2O$	10.45	62	60	1b, 3
$CsNi^{II}[Mn^{III}(CN)_6]\cdot H_2O$	10.42	54	42	1b
$Ni^{II}_3[Mn^{III}(CN)_6]_2\cdot 12H_2O$	10.29	42	30	1b
$Fe^{III}_4[Fe^{II}(CN)_6]_3\cdot xH_2O$	10.13	6.74	5.6	c
$Ni^{II}_3[Fe^{III}(CN)_6]_2\cdot xH_2O$	[b]	42.2	23	1c
$Cu^{II}_3[Fe^{III}(CN)_6]_2\cdot xH_2O$	[b]	13.0	20	1c

[a] Lattice constant. [b] Not reported. [c] Ito, A.; Suenaga, M.; Ono, K. *J. Chem. Phys.* **1968**, *48*, 3597. Buser, H. J.; Ludi, A.; Fischer, P.; Studach, T.; Dale, B. W. *Z. Phys. Chem.* **1974**, *92*, 354. Day, P.; Herren, F.; Ludi, A.; Gudel, H. U.; Hulliger, F.; Givord, D. *Helv. Chim. Acta* **1980**, *63*, 148.

ferromagnetic ordering at lower temperatures (Table 1). In contrast, Prussian blue structured materials with differing electronic structures, e.g., d^5 ($t_{2g}^3e_g^2$) and d^3 (t_{2g}^3) $CsMn^{II}[Cr^{III}(CN)_6]\cdot H_2O$ (T_c = 90 K),[5a] order ferrimagnetically. Many examples of Prussian blue structured ferrimagnets have been reported, and those with high T_c's include $CsMn^{II}[Cr^{III}(CN)_6]\cdot H_2O$ (T_c = 90 K),[5a] $Cs_2Ni[V(CN)_6]$ (T_c = 125 K),[1b] $Cr_{1.5}[Cr(CN)_6]\cdot 5H_2O$ (T_c = 240 K),[5b] $Cr^{III}[Cr^{III}(CN)_6]_{0.93}[Cr^{II}(CN)_6]_{0.05}$ (T_c = 260 K),[5c] and the room-temperature magnets: $V^{II/III}[Cr^{III}(CN)_6]_{0.86}\cdot 2.8H_2O$ (**1**) (T_c = 315 K),[5d] $V^{II/III}(V^{IV}O)_{0.02}[Cr^{III}(CN)_6]_{0.69}(SO_4)_{0.23}\cdot 3.0H_2O\cdot 0.02K_2SO_4$ (T_c = 310 K) (**2**),[5e] $Cs_{0.82}V^{II}_{0.66}(V^{IV}O)_{0.34}[Cr^{III}(CN)_6]_{0.92}(SO_4)_{0.203}\cdot 3.6H_2O$ (T_c = 315 K) (**3**),[5e] $K_{0.058}V^{II/III}[Cr^{III}(CN)_6]_{0.79}\cdot(SO_4)_{0.058}\cdot xH_2O$ (T_c = 372 K),[5f] and $KV^{II}[Cr^{III}(CN)_6]\cdot 2H_2O$ (T_c = 376 K).[5g] A recent addition to the vanadium−chromium family is $(V^{IV}O)[Cr^{III}(CN)_6]_{0.67}\cdot 3.3H_2O$ (T_c = 115 K), with structural refinement allowing an accurate estimation of the exchange-coupling parameter, J.[5h]

To eliminate the need for an auxiliary cation, as well as to minimize structural defects to maximize the number of nearest-neighbor ferromagnetic exchange pathways, $Ni^{II}[Mn^{IV}(CN)_6]$, isoelectronic with $CsNi^{II}[Cr^{III}(CN)_6]\cdot 2H_2O$,[3] was targeted for preparation. $Mn^{II}[Mn^{IV}(CN)_6]\cdot 1.4H_2O$ was reported to be a ferrimagnet with a T_c of 48.7 K,[6] suggesting that $M^{II}[Mn^{IV}(CN)_6]$ should also magnetically order with relatively high T_c's. Furthermore, $Ni^{II}[Mn^{IV}(CN)_6]$ with spins on adjacent sites in orthogonal orbitals should order ferromagnetically.[1−3] Because of the instability of aqueous $[Mn^{IV}(CN)_6]^{2-}$, an aprotic synthon was developed.[7] In addition to the ferromagnetic coupling expected for $Ni^{II}[Mn^{IV}(CN)_6]$, $M^{II}[Mn^{IV}(CN)_6]$ (M = Co, Mn, Cr, V) with high-spin d^7 Co^{II} ($t_{2g}^3e_g^2$), d^5 Mn^{II} ($t_{2g}^3e_g^2$), d^4 Cr^{II} ($t_{2g}^3e_g^1$), and d^3 V^{II} (t_{2g}^3) should exhibit antiferromagnetic coupling with d^3 Mn^{IV} (t_{2g}^3). The $Mn^{II}[Mn^{IV}(CN)_6]$ and $Cr^{II}[Mn^{IV}(CN)_6]$ compounds are expected to order as ferrimagnets, whereas $Fe^{II}[Mn^{IV}(CN)_6]$, $Co^{II}[Mn^{IV}(CN)_6]$, and $V^{II}[Mn^{IV}(CN)_6]$ may order as antiferromagnets with no net moment. $Fe[Mn(CN)_6]$ was initially studied; it exhibits a complex combination of electron transfer and linkage isomerization processes, and hence complex and variable stoichiometries and oxidation states.[8] Synthesis of this class of compounds in aprotic organic media can lead to highly disordered structures that undergo intermetallic electron transfer and exhibit unusual magnetic behavior, as was observed for the anhydrous $Fe[Mn(CN)_6]$.[8] Herein, we report the preparation and magnetic properties of $M[Mn(CN)_6]$ (M = V, Cr, Mn, Co, Ni) and electron transfer for M = V, Cr, and Mn, as well as the unexpected bulk magnetic behavior found in the Co- and V-containing compounds. These results are compared to those observed for $Fe[Mn(CN)_6]$,[8] as well as those for $Mn^{II}[Mn^{IV}(CN)_6]$ prepared from acid media.[6]

Experimental Section

All manipulations were performed under N_2 or Ar using a Vacuum Atmospheres inert-atmosphere DriLab. Dichloromethane was dried and distilled under N_2 from CaH_2; acetonitrile was dried and double-distilled under N_2 from CaH_2; tetrahydrofuran was dried and distilled under N_2 from sodium benzophenone ketyl radical. $[PPN]_2[M^{IV}(CN)_6]$[7] [PPN = $(Ph_3P)_2N$] and $[M^{II}(NCMe)_6]\{B[C_6H_3(CF_3)_2]_4\}_2$ (M = V, Cr, Mn, Co, Ni)[9] were made as previously reported. Great care was taken to keep these materials impurity-free with only the two metal constituents mixed together in freshly purified and dried solvents. All of the starting materials were crystalline, pure, fresh, and handled only in glass or plastic with Teflon-coated equipment.

Infrared spectra (±1 cm^{-1}) were taken on Nujol and Fluorolube mulls between NaCl plates and recorded on either a Perkin-Elmer model 783 or a BioRad model FTS-40 spectrophotometer with ±1 cm^{-1} resolution. X-ray powder diffraction spectra were taken on a Rigaku Miniflex diffractometer model 1GC2 (Cu Kα). Samples were mounted in a glovebox under a N_2 atmosphere on glass slides and contained in an airtight sample chamber with a Mylar window during data collection. The reflection 2θ values were corrected using an internal crystalline silicon standard, and refinements were made using a VAX-based refinement program, LATPARM.

X-ray photoelectron spectra (XPS) were obtained using a Fisons ESCALAB model 220i-XL spectrometer with an Al Kα radiation source operated at 10 kV and 15 mA. High-resolution scans were measured using a band-pass energy of 20 eV. The X-ray beam was focused to a 100-μm spot size while a 6- to 8-eV electron flood gun was used to control charging on the samples. System pressures were $\sim 7 \times 10^{-12}$ bar. The compounds were mounted on a stainless-steel holder with double-sided conducting tape in a glovebox and transferred under N_2 by a special transfer arm that allowed direct O_2-free loading of the sample into the spectrometer. The carbon 1s peak of the double-sided conducting tape (284.6 eV) was used as a reference for binding energy shifts in the spectra. Binding energies are determined to within ± 0.1 eV.

Electron paramagnetic resonance (EPR) spectra were obtained with a Bruker model ER 200D-SRC spectrometer equipped with an X-band microwave bridge, model ER 042 MRH. Measurements were made at ambient temperature and at 77 K using a liquid-N_2-immersion Dewar. Measurements were made on solids as powders contained in 1-mm fused-quartz capillary tubes contained in standard fused-quartz EPR tubes.

Thermal properties of material were studied on a TA Instruments model 2910 differential scanning calorimeter (DSC) and a TA model 2050 thermal gravimetric analyzer (TGA). The DSC is equipped with an LNCA liquid N_2 cooling accessory enabling operation between −150 and 725 °C. The TGA is also equipped with a TA-MS Fison triple-filter quadrupole mass spectrometer to identify gaseous products with masses less than 300 amu. The TGA operates between ambient and

(5) (a) Greibler, W. D.; Babel, D. *Z. Naturforsch* **1982** *87b*, 832. (b) Mallah, T.; Thiébaut, S.; Verdaguer, M.; Veillet, P. *Science* **1993**, *262*, 1554. (c) Buschmann, W. E.; Paulson, S. C.; Wynn, C. M.; Girtu, M.; Epstein, A. J.; White, H. S.; Miller, J. S. *Adv. Mater.* **1997**, *9*, 645; *Chem. Mater.* **1998**, *10*, 1386. (d) Ferlay, S.; Mallah, T.; Ouahes, R.; Veillet, P.; Verdaguer, M. *Nature* **1995**, *378*, 701. (e) Dujardin, E.; Ferlay, S.; Phan, X.; Desplanches, C.; Moulin, C. C. D.; Sainctavit, P.; Baudelet, F.; Dartyge, E.; Veillet, P.; Verdaguer, M. *J. Am. Chem. Soc.* **1998**, *120*, 11 347. (f) Hatlevik, Ø.; Buschmann, W. E.; Zhang, J.; Manson, J. L.; Miller, J. S. *Adv. Mater.* **1999**, *11*, 914. (g) Holmes, S.; Girolami, G. *J. Am. Chem. Soc.* **1999**, *121*, 5593. (h) Ferlay, S.; Mallah, T.; Ouahès, R.; Veillet, P.; Verdaguer, M. *Inorg. Chem.* **1999**, *38*, 229.

(6) Klenze, R.; Kanellakopulos, B.; Trageser, G.; Eysel, H. H. *J. Chem. Phys.* **1980**, *72*, 5819.

(7) Buschmann, W. E.; Vasquez, C.; Ward, M. D.; Jones, N. C.; Miller, J. S. *J. Chem. Soc. Chem., Commun.* **1997**, 409. This procedure was improved by using $[Fe(C_5H_5)_2]\{B[C_6H_3(CF_3)_2]_4\}$ as the oxidant in MeCN to give up to 90% yield.

(8) Buschmann, W. E.; Ensling, J.; Gütlich, P.; Miller, J. S. *Chem.—Eur. J.* **1999**, *5*, 3019.

(9) Buschmann, W. E.; Miller, J. S. *Chem.—Eur. J.* **1998**, *4*, 1731.

1000 °C and is located in a Vacuum Atmospheres inert-atmosphere DriLab to study oxygen- and moisture-sensitive samples. DSC samples were weighed and hermetically sealed in aluminum pans in an argon atmosphere. TGA samples were handled in an argon atmosphere and heated under a nitrogen purge. Sample sizes were in the range of 0.8 and 2 mg. Heating rates were 15 °C/min for TGA and 5 °C/min for DSC experiments.

Elemental analyses were performed on freshly prepared samples that were hermetically sealed under argon in tin capsules and combusted in a Perkin-Elmer model 2400 elemental analyzer. Vanadium pentoxide (LECO, Inc.) was added to samples as a combustion aid in some analyses. Nonetheless, incomplete combustion prevented any meaningful compositional information from being obtained.

Magnetic susceptibility measurements were made between 2 and 300 K using a Quantum Design MPMS-5 5T SQUID magnetometer with a sensitivity of 10^{-8} emu or 10^{-12} emu/Oe at 1 T and equipped with the ultralow field (~0.005 Oe), reciprocating sample measurement system, and continuous low-temperature control with enhanced thermometry features. Zero-field cooled (ZFC) measurements were made in a residual field of ca. -0.002 ± 0.001 to 0.002 ± 0.001 Oe based on the fluxgate response and measuring in a 5 kOe field upon warming, and are fit to the Curie−Weiss law, $\chi \propto (T - \theta)^{-1}$. Low field M($T$) (measured at 5 Oe upon warming) and M(H) (to 50 kOe) measurements are also made after cooling in zero field. The χ_{ac} measurements were made on samples cooled in zero field and measured upon warming in zero field with a 1 Oe ac-field amplitude at driving frequencies of 10, 100, and 1000 Hz. All measurements were made on powders contained in airtight Delrin holders supplied by Quantum Design. The data were corrected for the measured diamagnetism of each holder used. Core diamagnetism of $M[Mn(CN)_6]$ was calculated from standard diamagnetic susceptibility tables, giving a value of -78.4×10^{-6} emu/mol.

$V^{III}[Mn^{III}(CN)_6]$. A 10-mL, 1:1 THF/CH_2Cl_2 solution of $[V(NCMe)_6]\{B[C_6H_3(CF_3)_2]_4\}_2$ (0.7696 g, 0.3804 mmol) was added to a 10-mL CH_2Cl_2 solution of $[(Ph_3P)_2N]_2[Mn(CN)_6]$ (0.4900 g, 0.3804 mmol) while excluding light. A dark-blue-black, gel-like precipitate formed immediately. The solid was recovered by filtration and washed several times with CH_2Cl_2 and THF until the filtrate was colorless. The solid was dried in vacuo at room temperature for ca. 12 h. A blue-black solid was isolated in quantitative yield. IR ν_{CN} (Nujol): 2132 (m), 2091 (sh) cm^{-1}. Dec ~40 °C (DSC, T_{onset}), ~40 °C (TGA, T_{onset}).

$Cr^{III}[Mn^{III}(CN)_6]$. A 10-mL, 1:1 THF/CH_2Cl_2 solution of $[Cr(NCMe)_6]\{B[C_6H_3(CF_3)_2]_4\}_2$ (1.000 g, 0.4940 mmol) was added to a 10-mL CH_2Cl_2 solution of $[(Ph_3P)_2N]_2[Mn(CN)_6]$ (0.6364 g, 0.4940 mmol) while excluding light. A dark-brown, gel-like precipitate formed immediately. The solid was recovered by filtration and washed several times with CH_2Cl_2 and THF until the filtrate was colorless. The solid was dried in vacuo at room temperature for ca. 12 h. A dark-brown solid was isolated in quantitative yield. IR ν_{CN} (Nujol): 2137 (m) cm^{-1}. Dec ~30 °C (DSC, T_{onset}), ~40 °C (TGA, T_{onset}).

$Mn^{III}[Mn^{III}(CN)_6]$. A 10-mL, 1:1 THF/CH_2Cl_2 solution of $[Mn(NCMe)_6]\{B[C_6H_3(CF_3)_2]_4\}_2$ (1.000 g, 0.4933 mmol) was added to a 10-mL CH_2Cl_2 solution of $[(Ph_3P)_2N]_2[Mn(CN)_6]$ (0.6355 g, 0.4933 mmol) while excluding light. A dark-brown, gel-like precipitate formed immediately. The solid was recovered by filtration and washed several times with CH_2Cl_2 and THF until the filtrate was colorless. The solid was dried in vacuo at room temperature for ca. 12 h. A dark-brown solid was isolated in quantitative yield. IR ν_{CN} (Nujol): 2138 (m) cm^{-1}. Dec 92 °C (DSC, T_{onset}), 70 °C (TGA, T_{onset}).

$Co^{II}[Mn^{IV}(CN)_6]$. A 10-mL THF solution of $[Co(NCMe)_6]\{B[C_6H_3(CF_3)_2]_4\}_2$ (0.9500 g, 0.4674 mmol) was added to a 10-mL CH_2Cl_2 solution of $[(Ph_3P)_2N]_2[Mn(CN)_6]$ (0.6021 g, 0.4674 mmol) in darkness. A dark-brown, gel-like precipitate formed immediately. The solid was recovered by filtration and washed several times with CH_2Cl_2 and THF until the filtrate was colorless. The solid was dried in vacuo at room temperature for ca. 12 h. A dark-brown solid was isolated in quantitative yield. IR ν_{CN} (Nujol): 2167 (m) cm^{-1}. Dec 100 °C (DSC T_{onset}), 80 °C (TGA T_{onset}).

$Ni^{II}[Mn^{IV}(CN)_6]$. A 10-mL THF solution of $[Ni(NCMe)_6]\{B[C_6H_3(CF_3)_2]_4\}_2$ (1.100 g, 0.5413 mmol) was added to a 10-mL CH_2Cl_2 solution of $[(Ph_3P)_2N]_2[Mn(CN)_6]$ (0.6973 g, 0.5413 mmol) in darkness. A green-brown, gel-like precipitate formed immediately. The solid was recovered by filtration and washed several times with CH_2Cl_2 and THF until the filtrate was colorless. The solid was dried in vacuo at room temperature for ca. 12 h. An olive-green solid was isolated in quantitative yield. IR ν_{CN} (Nujol): 2155 (m) cm^{-1}. Dec. 91 °C (DSC, T_{onset}), 61 °C (TGA, T_{onset}).

Results and Discussion

$M[Mn(CN)_6]$ (M = Ni, Co, Mn, Cr, V) were made by mixing stoichiometric amounts of the corresponding $[M^{II}(NCMe)_6]\{B[C_6H_3(CF_3)_2]_4\}_2$ salts with $[PPN]_2[Mn^{IV}(CN)_6]$ in CH_2Cl_2/THF. The colored solids formed absorb moisture, but are moderately stable to moisture and oxygen, except for the V-containing compound that shows the formation of an oxidized vanadyl species according to IR analyses. These synthetic conditions were determined by evaluating the effect of several synthetic parameters, including various counterions and solvent types, on the products' physical and magnetic properties. The choice of materials presented in this report was determined on the basis of the following observations.

Preliminary attempts to prepare $M^{II}[Mn^{IV}(CN)_6]$ using $[M^{II}(NCMe)_6][X]_2$ {X = $[BF_4]^-$ or $[F_3CSO_3]^-$} as the cation sources in MeCN, led to the isolation of materials containing significant amounts (according to IR analyses) of coordinated MeCN, e. g., υ_{CN} 2308, 2283 cm^{-1} (Ni) and 2307, 2269 cm^{-1} (Co), and either coordinated $[BF_4]^-$ or $[F_3CSO_3]^-$, e. g., ν_{SO3} ~ 1310 cm^{-1} and ν_{CF3} ~ 1033 cm^{-1}.[10] The MeCN cannot be fully displaced by water when exposed to ambient moisture and, for the latter, $[PPN]^+$ is not present as the counterion (i.e., the M^{2+} cation must balance the charge), according to IR and X-ray photoelectron spectra (XPS) analyses. Heating the compounds in vacuo removes MeCN, but leads to decomposition. Additionally, the magnetic moment of these solids is consistent with two MeCN molecules per formula unit (vide infra), far more than can be accounted for from solely surface coordination. This finding suggests that some MeCN remains coordinated to the M^{2+} cation and blocks coordination sites from the $[Mn(CN)_6]^{2-}$ anion. Results of EPR studies are consistent with the above results, showing incomplete magnetic coupling as the presence of an uncoupled Mn^{4+} hyperfine structure for Ni- and $Co[Mn(CN)_6]$, vide infra. The low field magnetization versus temperature studies reveal two transitions in these materials, suggesting the presence of more than one magnetic phase in these solids. These undesirable properties led to the study of materials made from THF/CH_2Cl_2 that do not exhibit these particular complications.

Each of the studied compounds is valence-ambiguous because they can be formulated as either $M^{II}[Mn^{IV}(CN)_6]$ or $M^{III}[Mn^{II}(CN)_6]$, the latter requiring an electron-transfer process. The assignment of oxidation states was determined from infrared and XPS studies.

Infrared Spectra. $M[Mn(CN)_6]$ (M = Cr, Mn, Co, Ni) exhibit a single, broad ν_{CN} absorption ranging from 2137 (M = Cr) to 2167 cm^{-1} (M = Co) of medium intensity (Table 2). When M = V, there is an additional broad, weak shoulder (~2091 cm^{-1}) on the low-energy side of the primary absorption (2132 cm^{-1}). There is also evidence for trace amounts of THF in the IR with a weak, characteristic absorption between ca. 1029 and 1034 cm^{-1}. However, THF, unlike MeCN, is fully displaced by water upon exposure to moisture. Trace amounts of the $[PPN]\{B[C_6H_3(CF_3)_2]_4\}$ byproduct are also detected and are difficult to remove, even after multiple washings with clean solvent, because of the extremely fine particle size of the powders. The materials reported herein are the cleanest samples obtained on the basis of the IR data.

Table 2. Characteristic Infrared ν_{CN} Absorption Peak Maxima[a] and Color of THF/CH_2Cl_2-Prepared M[Mn(CN)$_6$] (M = V, Cr, Mn, Fe, Co, Ni)

M	ν_{CN} (cm^{-1})	color
V	2132 m (~2091 sh)	blue-black
Fe	2127 m[8]	dark green[8]
Cr	2137 m	dark brown
Mn	2138 m	dark brown
Co	2167 m	dark brown
Ni	2155 m	olive-green

[a] Nujol mulls between NaCl windows; medium (m), shoulder (sh).

The M = V, Cr, and Mn materials have ν_{CN} absorption values between 2134 ± 2 cm^{-1} falling within the 2125 to 2050 cm^{-1} range known for Prussian blue analogues containing $[Mn^{III}(CN)_6]^{3-}$.[8,15] Hence, the oxidation states in M[Mn(CN)$_6$] (M = V, Cr, Mn) are assigned as $M^{III}[Mn^{III}(CN)_6]$ arising from an electron transfer from the cationic *N*-bound M^{2+} center to the anionic *C*-bound $[Mn^{IV}(CN)_6]^{2-}$. Electron transfer is also observed for Fe[Mn(CN)$_6$] (2142 cm^{-1}).[8] It is not surprising that V^{II} and Cr^{II} are easily oxidized by $[Mn^{IV}(CN)_6]^{2-}$ ($Mn^{IV/III}$ $E_{1/2}$ = +0.14 V vs SCE).[7] It is curious, however, that the reaction of Mn^{II} and $[Mn^{IV}(CN)_6]^{2-}$ in anhydrous organic media always forms $Mn^{III}[Mn^{III}(CN)_6]$, whereas in aqueous media the disproportionation of $[Mn^{III}(CN)_6]^{3-}$ results in the formation of $Mn^{II}[Mn^{IV}(CN)_6]$.[6] The 2091-cm^{-1} low-energy ν_{CN} shoulder observed in V[Mn(CN)$_6$] is consistent with the presence of $[Mn^{II}(CN)_6]^{4-}$, whose known ν_{CN} absorption values are below 2100 cm^{-1} [12b] and may be due to a small amount of further-reduced Mn^{II} with some V^{IV} present, although this could not be confirmed.

The M = Co (2167 cm^{-1}) and Ni (2155 cm^{-1}) materials have ν_{CN} absorption values that exceed the known range for $[Mn^{III}(CN)_6]^{3-}$-containing Prussian blue analogues, but are not as great as for $Mn^{II}[Mn^{IV}(CN)_6]$ (ν_{CN} = 2183 cm^{-1}).[6] A 20- to 100-cm^{-1} increase in the ν_{CN} band is expected upon coordination of the nitrogen end of cyanide of the free hexacyanometalate ion.[11,16] The ν_{CN} value of 2132 cm^{-1} for $(PPN)_2[Mn^{IV}(CN)_6]$[7] gives $M^{II}[Mn^{IV}(CN)_6]$ a minimum expected ν_{CN} absorption at 2152 cm^{-1} upon complexation and leads to the assignment of $M^{II}[Mn^{IV}(CN)_6]$ oxidation states for M = Co, Ni. XPS analysis and magnetic susceptibility measurements independently confirmed these oxidation state assignments, vide infra.

M[Mn(CN)$_6$] (M = Cr, Mn, Co, Ni) show no significant changes in their ν_{CN} absorption bands upon exposure to moisture or with heating below their decomposition temperatures. The primary ν_{CN} absorption of V[Mn(CN)$_6$] at 2132 cm^{-1}, the broadest in the series, rapidly shifts to 2148 cm^{-1} upon exposure to air with a gradual growth of a $\upsilon_{V=O}$ peak observed ca. 1000 cm^{-1}. This increase in ν_{CN} due to the formation of V^{IV}=O is also observed for several reported V[Cr(CN)$_6$] materials.[5d-g] For all cases of M[Mn(CN)$_6$] above, in the absence of O_2, there is no evidence to suggest the presence of dynamic changes (i.e., oxidation state, linkage isomerization) as are found for Fe[Mn(CN)$_6$].[8]

Table 3. XPS Data of M[Mn(CN)$_6$] (M = Ni, Co)] and Model Hexacyanomanganate Salts

		Binding Energy (eV)[a]			
	N	anion, $[Mn(CN)_6]^{n-}$		cation	
compound	1s	$2p_{1/2}$	$2p_{3/2}$	$2p_{1/2}$	$2p_{3/2}$
$K_3[Mn^{III}(CN)_6]$	397.6	653.5	641.6	294.7	292.6 (K^+)
$[PPN]_3[Mn^{III}(CN)_6]$	397.2	652.6	640.6	132.7	(P 2p)
$[PPN]_2[Mn^{IV}(CN)_6]$	398.2	654.5	642.8	133.2	(P 2p)
Ni[Mn(CN)$_6$]	398.2	654.1	642.0	873.1	855.2 (Ni)
Co[Mn(CN)$_6$]	398.2	654.0	642.1	797.1	782.2 (Co)

[a] Spectra were normalized on the *C* 1s peak at 284.6 eV.

XPS Analysis. XPS studies were undertaken to confirm the metal oxidation states in M[Mn(CN)$_6$] (M = Ni, Co) (Table 3). The observed binding energies of the Mn $2p_{3/2}$ electrons are 642.0 eV for Ni[Mn(CN)$_6$] and 642.1 eV for Co[Mn(CN)$_6$], while the $2p_{3/2}$ binding energies are 855.2 eV for Ni and 782.2 eV for Co. These Mn $2p_{3/2}$ values are consistent with those found for $[PPN]_2[Mn^{IV}(CN)_6]$ (642.8 eV) and greater than the Mn $2p_{3/2}$ peaks found for $[PPN]_3[Mn^{III}(CN)_6]$ (640.6 eV) and $K_3[Mn^{III}(CN)_6]$ (641.6 eV). The reported $2p_{3/2}$ values from tabulated standards for $Ni(NH_3)_6^{2+}$ complexes range from 855.9 to 856.5 eV,[17] supporting the oxidation state assignment in Ni[Mn(CN)$_6$]. The range of reported $2p_{3/2}$ values for Co^{II} complexes in a weak-field ligand environment vary widely, between 780.1 eV {$(Et_4N)_2[CoBr_4]$} and 784.0 eV [$Co(SO_4)$], overlapping the range of values for Co^{III} [17] and thus providing no additional diagnostic information.

Thermal Stability. The thermal properties of M[Mn(CN)$_6$] (M = V, Cr, Mn, Co, Ni) were evaluated by TGA/DSC. Generally, each compound shows the onset of a decompositional weight loss in the TGA above ca. 40 °C, corresponding to the loss of cyanide radicals in the form of cyanogen as found for Fe[Mn(CN)$_6$].[8] The first broad weight-loss step corresponds to the loss of approximately two CNs, followed by further decomposition at higher temperatures (>300 °C), resulting in black residues. The one exception is Mn[Mn(CN)$_6$], which has an additional sharp ~8% weight loss at 233 °C (T_{onset}), corresponding to the loss of approximately one more CN before further losses above 400 °C. The DSC of each compound shows a weak to very weak, broad exotherm beginning at ~90 °C (this exotherm is much greater for Co[Mn(CN)$_6$]) that corresponds to the first weight loss in the TGA. As decomposition continues at higher temperatures, a large amount of exothermic heat flow occurs in the DSC cell. Overall, these compounds are not very thermally stable, having a facile loss of cyanide from the $[Mn(CN)_6]^{n-}$ species as cyanogen in a manner similar to the thermolysis of $[Mn^{IV}(CN)_6]^{2-}$ to produce $[Mn^{II}(CN)_4]^{2-}$.[18]

X-ray Diffraction. The observed reflections in the powder X-ray diffraction patterns for M[Mn(CN)$_6$] (M = V, Cr, Mn, Co, Ni) are very broad, but regions of diffraction intensity are consistent with the most intense diffraction peaks expected for an fcc Prussian blue-type structure (Figure 1). A typical X-ray diffraction pattern for fcc Prussian blue (Figure 1a) made by a standard method[19] in aqueous media is included for comparison. $Ni^{II}[Mn^{IV}(CN)_6]$ prepared from $[Ni^{II}(NCMe)_6](F_3CSO_3)_2$ in MeCN (Figure 1b) retains some lattice order or moderate distribution of Ni−Mn spacings shown by the broad reflections.

(10) Lawrence, G. A. *Chem. Rev.* **1986**, *86*, 17.
(11) Dunbar, K. R.; Heintz, R. A. In *Progress in Inorganic Chemistry*; Karlin, K. D., Ed.; John Wiley: New York, 1997; Vol. 45, p 288.
(12) (a) Sharpe, A. G. *The Chemistry of Cyano Complexes of the Transition Metals*; Academic Press: New York, 1976. (b) Sharpe, A. G. *The Chemistry of Cyano Complexes of the Transition Metals*; Academic Press: New York, 1976, Chapter 6.
(13) Fowler, J. R.; Kleinberg, J. *Inorg. Chem.* **1970**, *9*, 1005.
(14) Buschmann, W. E.; Liable-Sands, L.; Rheingold, A. L.; Miller, J. S. *Inorg. Chim. Acta* **1999**, *284*, 175.
(15) Ently, W. R.; Girolami, G. S. *Inorg. Chem.* **1994**, *33*, 5165; **1995**, *34*, 2262.
(16) Jones, L. H.; Swanson, B. I. *Acc. Chem. Res.* **1976**, *9*, 128.
(17) Moulder, J. F.; Stickle, W. F.; Sobol, P. E.; Bomben, K. D. *Handbook of X-ray Photoelectron Spectroscopy*; Chastain, J., King, R. C., Jr., Eds.; Physical Electronics: Eden Prairie, MN, 1995.
(18) Buschmann, W. E.; Arif, A. M.; Miller, J. S. *Angew. Chem., Int. Ed. Engl.* **1998**, *37*, 781.
(19) Beall, G. W.; Milligan, W. O.; Korp, J.; Bernal, I. *Inorg. Chem.* **1977**, *16*, 2715.

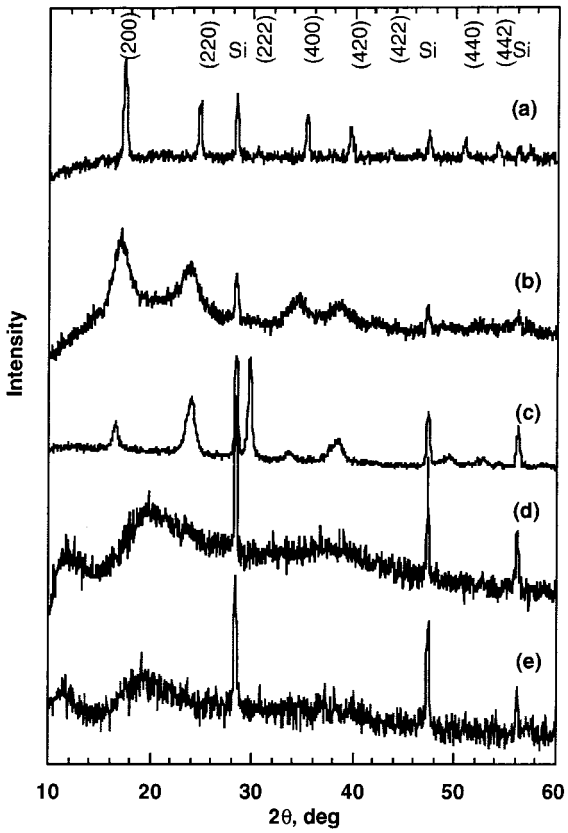

Figure 1. X-ray powder diffraction patterns of (a) Prussian Blue, $Fe_4[Fe(CN)_6]_3 \cdot 14H_2O$, (b) $Ni[Mn(CN)_6] \cdot 2MeCN$, (c) $Co[Mn(CN)_6] \cdot 2MeCN$, (d) $Ni[Mn(CN)_6]$, and (e) $Co[Mn(CN)_6]$. Silicon is used as an internal standard.

Table 4. Lattice Constants for THF/CH_2Cl_2-Prepared $M[Mn(CN)_6]$ (M = V, Cr, Mn, Fe, Co, Ni)

compound	solvent	*a*, Å
$V^{III}[Mn^{III}(CN)_6]$	THF/CH_2Cl_2	9.3(3)
$Cr^{III}[Mn^{III}(CN)_6]$	MeCN	10.57(4)
	THF/CH_2Cl_2	9.5(1)
$Mn^{III}[Mn^{III}(CN)_6]$	MeCN	10.65(1)
	THF/CH_2Cl_2	9.2(1)
$Mn^{II}[Mn^{IV}(CN)_6]$	H_2O	10.731(2)[6]
$Fe^{II}[Mn^{IV}(CN)_6]$	MeCN	10.50(2)[8]
	THF/CH_2Cl_2	9.6(1)[8]
$Co^{II}[Mn^{IV}(CN)_6]$	MeCN	10.40(2)
	THF/CH_2Cl_2	9.1(1)
$Ni^{II}[Mn^{IV}(CN)_6]$	MeCN	10.38(2)
	THF/CH_2Cl_2	9.0(1)

This pattern is representative of the patterns seen for $M[Mn(CN)_6]$ (M = Cr, Mn, Ni) made from MeCN. $Co^{II}[Mn^{IV}(CN)_6]$ prepared from $[Co^{II}(NCMe)_6](BF_4)_2$ in MeCN (Figure 1c) has an inverted intensity pattern, with the (222) reflection intensity being greatest. All compounds made from MeCN can be refined within the *Fm*3*m* space group, giving unit cell parameters, *a*, ranging from 10.38 to 10.65 Å (Table 4). These fall within the typical range of *a*-values observed for the Prussian blue analogues, 10.1 to 10.8 Å.[1,3−5,19]

$Ni^{II}[Mn^{IV}(CN)_6]$ made from $[Ni^{II}(NCMe)_6]\{B[C_6H_3(CF_3)_2]_4\}_2$ in CH_2Cl_2/THF (Figure 1d) diffracts very poorly, and its broad reflections are representative of the entire series of anhydrous Prussian blue materials reported here (M = V, Cr, Mn, Co, Ni) as well as $Fe[Mn(CN)_6]$.[8] The poor diffraction quality of these compounds makes the determination of *a* rather approximate, but values of *a* range from 9.0 to 9.5 Å (Table 3). These values are determined from the *d* spacing of the low-angle peak maxima. The reduced *a*-values are attributed to a contraction of the lattice (M−Mn spacing) in the absence of water or some well-coordinating solvent molecule (i.e., MeCN) that is necessary to help stabilize the structure during lattice formation. This contraction is observed in a structural study of $Mn_3[Co(CN)_6]_2 \cdot 12H_2O$ showing that hydrogen bonding of zeolitic water plays a major role in stabilizing the fcc lattice, and that the *a* decreases from 10.44 to 10.22 Å and the diffraction peaks become very diffuse upon dehydration.[19] The presence of empty cavities within a Prussian blue structural framework leads to an unstable state relative to the entropy gained upon filling that space.[20] For CH_2Cl_2/THF-prepared compounds, the ordered Prussian blue type lattices are inherently unstable, with the vacant pore space resulting in significant crystallographic disorder. The following particle size estimation and ac-susceptibility studies (vide infra) also support the presence of lattice disorders.

The broadening of the X-ray diffraction peaks can be related not only to the degree of crystallinity, but also to the crystallite size. In an ordered solid, crystallites greater than ∼2000 Å in diameter, assuming spheres, give sharp, narrow diffraction peaks, e.g., Figure 1a (i.e., for a crystal containing 2000 planes with *d* spacing of 1 Å). Below ∼2000 Å the peakwidth is approximately related to the crystallite size according to Scherrer formula,[21] $t = 0.9\lambda/(B \cos \theta_B)$ (*t* is the crystal thickness (in Å), λ is the X-ray wavelength (in Å), and θ_B is the Bragg angle (in radians); the line broadening, *B*, is a measure of the extra peakwidth at half-height obtained from the Warren formula, $B = [B_M^2 - B_S^2]^{1/2}$, where B_M is the measured half-height peakwidth of the sample and B_S is the corresponding half-height peakwidth of an internal standard, i.e., Si, whose crystal size is greater than 2000 Å), the estimated particle sizes for the CH_2Cl_2/THF-prepared compounds are unreasonably small, ca. 15 Å. Particles approximately one to two unit cells in size are far too small to have long-range magnetic interactions (vide infra), as is the case for superparamagnets,[22] rendering the observed bulk magnetic ordering an impossibility. The broadening of the X-ray diffraction peaks is therefore attributed to a significant contribution from lattice disorder and a less dramatic reduction in particle size. One structural parameter that has been shown to vary is the linearity of the CN bridge between metal centers. A Cr−C−N and V−N−C angle of 168° is reported for $(V^{IV}O)[Cr^{III}(CN)_6]_{0.67} \cdot 3.3H_2O$ as well as a slightly distorted $[Cr^{III}(CN)_6]^{3+}$ octahedron.[5h] Such distortions may contribute to lattice contraction in these materials.

Thus, in the nonaqueous systems studied here, the ordered Prussian blue-type lattices are inherently unstable, with vacant pore space resulting in significant crystallographic disorder. This instability leads to important ramifications regarding the magnetic properties.

EPR. The $M[Mn(CN)_6]$ (M = Ni, Co) exhibit a single, very broad resonance ($\Delta H_{pp} \approx 680$ G) centered at $g = 2.02(1)$ at 77 K with no ^{55}Mn ($I = 5/2$) hyperfine structure; a representative spectrum is shown in Figure 2. This is characteristic of a magnetically coupled material above its critical temperature, T_c, where dipolar broadening dominates the relaxation processes.[23] If the EPR-active $S = 3/2$ Mn^{IV} ion is not present {i.e., Ni^{III}- or $Co^{III}[Mn^{III}(CN)_6]$ is present} a signal is unlikely to be observed

(20) This condition complies with the second law of thermodynamics.
(21) West, A. R. *Solid State Chemistry and Its Applications*; John Wiley: New York, 1984; pp 173−175.
(22) Palacio, F. In *Molecular Assemblies to the Devices: NATO Advanced Studies Workshop*; Coronado, E., Delhaès, P., Gatteschi, D., Miller, J. S., Eds.; Kluwer Academic Publishers.: Boston, 1996; Vol. E321, pp 51−55.

Table 5. Summary of the Magnetic Properties for THF/CH_2Cl_2-Prepared $M[Mn(CN)_6]$ (M = V, Cr, Mn, Fe, Co, Ni)

compound	θ (K) (T > 250 K)	T_c (K) (dc)	T_c (K) (ac, 10 Hz)	ϕ	H_{cr} (Oe)	M (emuOe/mol) (at 50 kOe)	M_r (at 0 kOe)
$V^{III}[Mn^{III}(CN)_6]$	−370	28	19	0.021	340[a]	2120[a]	40[a]
$Cr^{III}[Mn^{III}(CN)_6]$	−140	22	16	0.033	130[a]	5050[a]	80[a]
$Mn^{II}[Mn^{IV}(CN)_6]$[c]	−52	48.7	[e]	[e]	[e]	10 680[d]	[e]
$Mn^{III}[Mn^{III}(CN)_6]$	−105	31	27	NA	8[a]	16 840[a]	1500[a]
$Co^{II}[Mn^{IV}(CN)_6]$	−55	5.8	<1.75	NA	9[b]	9630[b]	4[b]
$Fe^{II}[Mn^{IV}(CN)_6]$[9]	−8	22	15.0	0.017	3[a]	21 600[a]	220[a]
$Ni^{II}[Mn^{IV}(CN)_6]$	−120	10	4.8	0.05	220[b]	8930[b]	250[b]

[a] 5 K. [b] 2 K. [c] 1.4 H_2O[6]. [d] 4.2 K. [e] Not reported in ref 6.

Table 6. Observed and Calculated Spin-Only $g = 2$ Effective Moments, μ_{Eff}, for THF/CH_2Cl_2-Prepared $M[Mn(CN)_6]$ (M = V, Cr, Mn, Fe, Co, Ni)

M	μ_{eff} (μ_B) obs	μ_{eff} (μ_B) calc $M^{III}[Mn^{III}(CN)_6]$ (high-spin M^{III})	μ_{eff} (μ_B) calc $M^{III}[Mn^{III}(CN)_6]$ (low-spin M^{III})	μ_{eff} (μ_B) calc $M^{II}[Mn^{IV}(CN)_6]$ (high-spin M^{II})	μ_{eff} (μ_B) calc $M^{II}[Mn^{IV}(CN)_6]$ (low-spin M^{II})
V	3.71	4.00	4.00	5.48	5.48
Cr	4.62	4.80	4.80	6.24	4.80
Mn	5.91	5.66	4.00	7.07	4.24
Fe[7]	6.51	6.56	3.32	6.24	3.87
Co	4.54	5.66	2.83	5.48	4.24
Ni	4.91	4.80	3.32	4.80	4.80

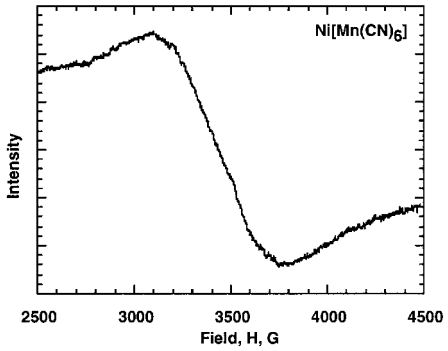

Figure 2. EPR spectrum at 77 K for $Ni[Mn(CN)_6]$, $g = 2.02$ (9.70 GHz).

at this temperature. An EPR signal is not observed for the Mn-containing compound that is presumed to be $Mn^{III}[Mn^{III}(CN)_6]$. The Ni- and Co-containing compounds made in MeCN exhibit a six-line ^{55}Mn ($I = 5/2$) hyperfine structure {|A| ≈ 90 G} superimposed on the broad 77 K EPR signal at $g \approx 2.02$ ($\Delta H_{pp} \approx 680$ G) due to incomplete magnetic coupling to $[Mn^{IV}(CN)_6]^{2-}$.[23] This presumably is due to excess coordinated MeCN and/or $[BF_4]^-$ or $[F_3CSO_3]^-$ that retain coordination sites on the M^{2+} cations, according to IR,[9,10] preventing full coordination of $[Mn^{IV}(CN)_6]^{2-}$, demonstrating the necessity of using more weakly coordinating solvents and counterions.

Magnetic Susceptibility. The temperature dependencies of the magnetic susceptibility, $\chi(T)$, of CH_2Cl_2/THF-prepared $M[Mn(CN)_6]$ (M = V, Cr, Mn, Co, Ni) were determined between 2 and 300 K, and the data above 250 K can be fit to the Curie−Weiss expression, $\chi \propto (T - \theta)^{-1}$, with θ-values ranging from −52 (M = Mn) to −370 K (M = V) (Table 5, Figure 3). The large negative values indicate strong antiferromagnetic coupling for this family of materials. The room-temperature effective moments, μ_{eff}, $[= 8\chi T]^{1/2}$, which range from 3.71 (M = V) to 5.91 μ_B (M = Mn), are within the range expected for these ions, consistent with the oxidation state assignments (Table 6).

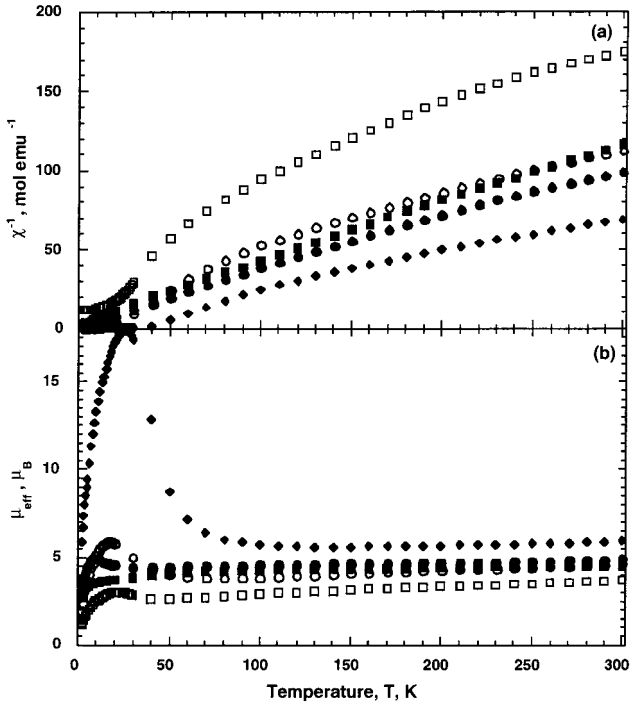

Figure 3. $1/\chi$ (a) and μ_{eff} (b) vs temperature for $M[Mn(CN)_6]$, [M = Ni (●), Co (■), at 2 K, and M = Mn (◆), Cr (○), V (□) at 5 K]. Samples are cooled in zero field to 2 K and data taken upon warming in a 5 kOe-applied field.

In addition to the negative θ-values, these compounds exhibit the onset of magnetic order, hysteresis, incomplete magnetic saturation at 50 kOe, and frequency-dependent $\chi'(T)$ and $\chi''(T)$ components in the ac-susceptibility (χ_{ac}) (Table 5). These results are qualitatively reproducible between samples, but have some variance in the transition temperatures and absolute magnetization values due to the issues of disorder and purity discussed above.

$Ni^{II}[Mn^{IV}(CN)_6]$. $Ni^{II}[Mn^{IV}(CN)_6]$ has a room-temperature effective moment, μ_{eff}, which at 4.91 μ_B is slightly higher than the predicted spin-only value of 4.80 μ_B for an uncoupled $S = 1$ (Ni^{II}) and 3/2 (Mn^{IV}) system with the EPR-determined 2.02(1) Landé g-value. The higher value is a consequence of the

(23) Bencini, A.; Gatteschi, D. *Electron Paramagnetic Resonance of Exchange Coupled Systems*; Springer-Verlag: New York, 1990; Chapter 6.

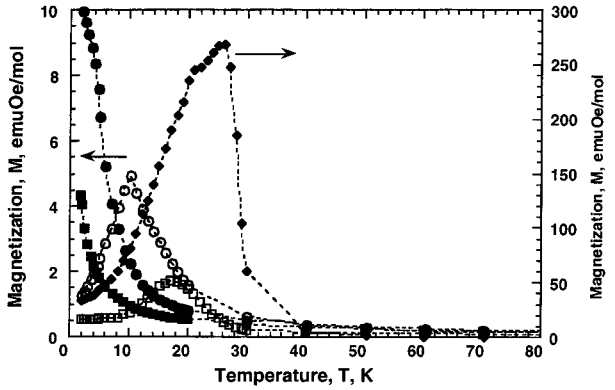

Figure 4. Low field temperature-dependent magnetization for M[Mn(CN)$_6$] [M = Ni (●), Co (■), at 2 K, and M = Mn (◆), Cr (○), V (□) at 5 K]. Samples are cooled in zero field to 2 K and data taken upon warming in a 5 Oe-applied field.

admixture of Ni^{II}'s first $^3T_2$ excited state possessing a second-order spin−orbit (Zeeman) effect with the $^3A_2$ ground state which increases its room temperature μ_{eff},[24] as also observed for the [Ni^{II}(NCMe)$_6$]{B[C$_6$H$_3$(CF$_3$)$_2$]$_4$}$_2$[9] and other Ni^{II} complexes.[9,24,25] Above 250 K the susceptibility can be fit to the Curie−Weiss expression with $\theta = -120$ K, indicating that strong antiferromagnetic coupling dominates the short-range exchange.

The low field (5 Oe) magnetization of Ni^{II}[Mn^{IV}(CN)$_6$] shows the onset of magnetic order below 10.3 K (by extrapolation of the steepest slope to M = 0, Figure 4). The $\chi_{ac}(T)$ data show both χ' (absorptive) and χ'' (dispersive) components of the magnetization (Figure 5a). There is frequency dependence in the $\chi_{ac}(T)$ response, indicative of spin-glass behavior.[26] The ordering temperature, T_c, is taken as the 10-Hz χ' peak maximum at 4.8 K. The field-dependent magnetization at 2.0 K has a steep initial slope below 10 kOe, and reaches 8930 emuOe/mol at 50 kOe, but does not saturate (Figure 6). The presence of $\chi''(T)$ suggests that this compound has a noncompensated moment and should exhibit hysteresis. The 2.0 K M(H) data between ±20 kOe show a coercive field, H_{cr}, of 220 Oe, and remanent magnetization of 250 emuOe/mol (Figure 7a).

From the above data, Ni^{II}[Mn^{IV}(CN)$_6$] orders as a bulk spin-glass-like ferrimagnet rather than an expected ferromagnet for Ni^{II} ($t_{2g}^6e_g^2$) coupled with [Mn^{IV}(CN)$_6$]$^{2-}$ (t_{2g}^3) due to ferromagnetic coupling among spins on adjacent sites in orthogonal orbitals.[2a,3] The large degree of structural disorder, evident in the X-ray diffraction experiments, results in the breakdown of strict geometric orbital orthogonality and introduces site/bond disorder and spin frustration (competing ferro- and antiferromagnetic interactions) that lead to spin-glass-like behavior as discussed below. This disorder also leads to a reduction of the ordering temperature despite the large θ-value that is indicative of strong short-range coupling. Disorder reduces the number

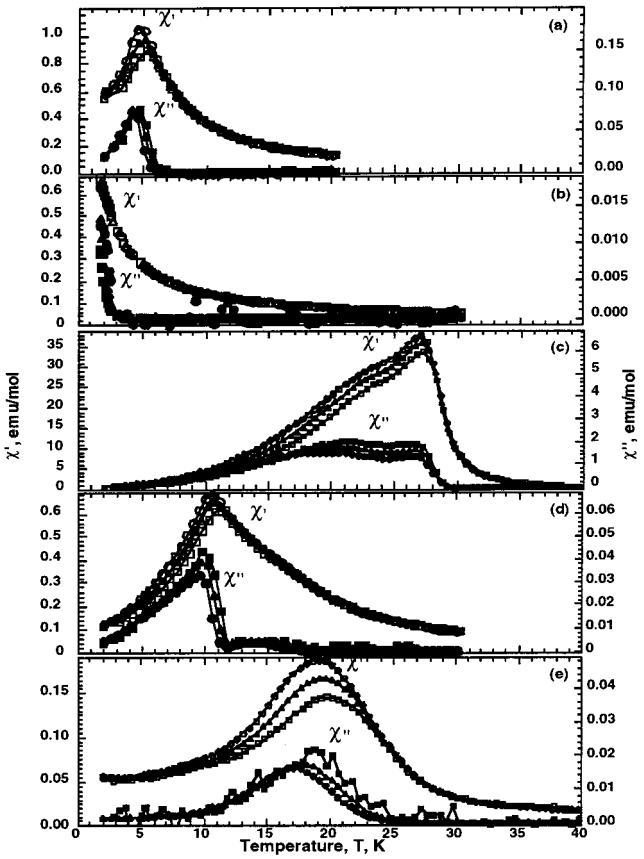

Figure 5. ac-χ vs temperature for M[Mn(CN)$_6$]: (a) M = Ni, (b) M = Co, (c) M = Mn, (d) M = Cr, (e) M = V at 10 Hz (○), 100 Hz (Δ), and 1000 Hz (■). Samples are cooled in zero field to 2 K and data taken upon warming with a 1 Oe ac field in zero-applied dc field.

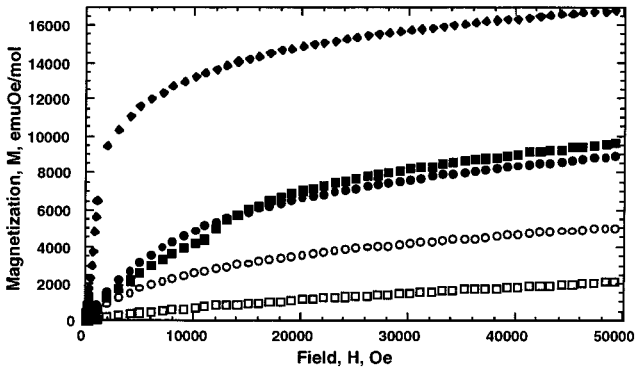

Figure 6. Magnetization vs field data for M[Mn(CN)$_6$] [M = Ni (●), Co (■), at 2 K, and M = Mn (◆), Cr (○), V (□) at 5 K]. Samples are cooled in zero field to 2 K.

and/or uniformity of cyanide linkages (i.e., exchange pathways) between metal centers. In Ni^{II}[Mn^{IV}(CN)$_6$], strong coupling can still exist between nearest neighboring ions; however, without a fully coupled lattice and uniform long-range structural order in all three dimensions, the long-range magnetic ordering will be disrupted and T_c reduced. This is the case throughout this entire series of M[Mn(CN)$_6$] materials.

Co^{II}[Mn^{IV}(CN)$_6$]. Co^{II}[Mn^{IV}(CN)$_6$] has a room-temperature μ_{eff} of 4.54 μ_B, which exceeds the predicted $g = 2$ spin-only value of 4.24 μ_B for an uncoupled $S = 1/2$ (low-spin Co^{II}) and 3/2 (Mn^{IV}) system, but is substantially less than the 5.48 μ_B expected for uncoupled $S = 3/2$ (high-spin Co^{II} and 3/2 Mn^{IV}) spins. (The predicted moment for uncoupled $S = 2$ (high-spin Co^{III}) and $S = 1$ (low-spin Mn^{III}) spins is 5.66 μ_B, which also

(24) (a) Figgis, B. N. In *Comprehensive Coordination Chemistry*; Wilkinson, G., Ed.; Pergamon: New York, 1987; Vol. 1, pp 259−274. (b) Carlin, R. L. *Magnetochemistry*; Springer-Verlag: New York, 1981; p 28.

(25) (a) Manson, J. L.; Kmety, C.; Huang, R. Q.; Lynn, J. W.; Bendele, G. M.; Pagola, S. P.; Stephens, W.; Liable-Sands, L.; Rheingold, A. L.; Epstein, A. J.; Miller, J. S. *Chem. Mater.* **1998**, *10*, 2552. (b) Hathaway, B. J.; Hola, D. G. *J. Chem. Soc.* **1964**, 2400. (c) Hathaway, B. J.; Hola, D. G.; Underhill, A. E. *J. Chem. Soc.* **1962**, 2444.

(26) (a) Mydosh, J. A. *Spin Glasses*; Taylor and Francis: Washington, DC, 1993; Chapter 1. (b) Mydosh, J. A. *Spin Glasses*; Taylor and Francis: Washington, DC, 1993; Chapter 3. (c) Ramirez, A. P. *Annu. Rev. Mater. Sci.* **1994**, *24*, 453. (d) O'Connor, C. J. In *Research Frontiers in Magnetochemistry*; O'Connor, C. J., Ed.; World Scientific: River Edge, NJ, 1993; pp 109−137.

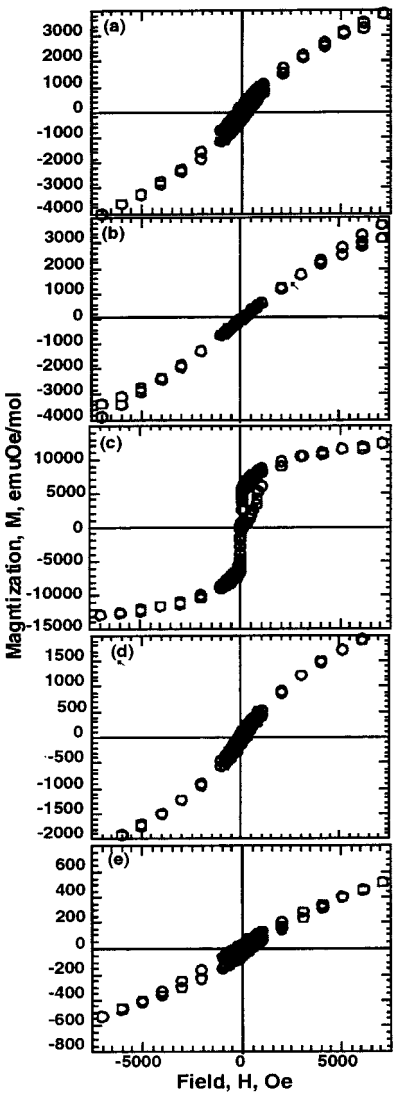

Figure 7. Hysteresis loops for M[Mn(CN)$_6$] at 2 K, (a) M = Ni, (b) M = Co; and 5 K, (c) M = Mn, (d) M = Cr, (e) M = V. Samples were cooled in zero field to 2 K.

exceeds the observed value.) The observed moment is expected to exceed the spin-only value, as zero field splitting for either the low-spin ^{2}E or the high-spin ^{4}T$_1$ ground states is significant. Values of μ_{eff} for high-spin Co^{II} compounds are typically in the range of 4.7 to 5.5 μ_B (3.87 μ_B spin-only value).[9,24,25c]

The $\mu_{eff}(T)$ gradually decreases with decreasing temperature down to ca. 75 K then decreases more rapidly down to ca. 15 K, below which it rapidly falls off (Figure 3b). The observed $\mu_{eff}(T)$ above 15 K is indicative of significant Zeeman effects, strong magnetic coupling (non-Curie behavior),[24] and antiferromagnetic coupling.[1c,27] The extrapolated θ-value of -55 K suggests that antiferromagnetic coupling dominates the short-range exchange. The rapid decrease in $\mu_{eff}(T)$ below 15 K suggests the onset of antiferromagnetic order; however, the low field magnetization shows a spontaneous ferro- or ferrimagnetic ordering below 5.8 K (Figure 4). The existence of both $\chi'(T)$ and $\chi''(T)$ is consistent with the presence of some ferromagnetic ordering (Figure 5b). A peak in $\chi'(T)$ could not be resolved above 1.75 K, but some frequency dependence is resolved in $\chi''(T)$, suggesting that there is some "glassy" behavior in Co^{II}[Mn^{IV}(CN)$_6$]. The field-dependent χ measurements at 2.0 K between $\pm$20 kOe show a small coercive field, H_{cr}, of 9 Oe, and remanent magnetization of 4 emuOe/mol (Figure 7b) further supporting the presence of magnetic order. The magnetization, however, does not fully saturate at 50 kOe (Figure 6).

The room-temperature μ_{eff} and long-range order observed for Co^{II}[Mn^{IV}(CN)$_6$] are both consistent with the presence of low-spin n Co^{II}. There is no example of a low-spin Co^{II} compound octahedrally coordinated by the nitrogen of six nitriles or cyanides. However, distortions in the ligand field arising from structural disorder, such as a missing nitrile linkage, will reduce the orbital symmetry from octahedral. This reduction leads to a distorted d-orbital manifold that appears, in this case, to stabilize a low-spin configuration. This condition produces a ground state that cannot be described as ^{2}E or ^{4}T$_1$. Lower orbital symmetry does lead to different electronic ground states that can give both high- and low-spin configurations as found in some Schiff base complexes.[28,29]

The 2 K magnetization at 50 kOe of 9630 emuOe/mol is additional evidence for a significant amount of uncompensated spin at low temperature. A saturation value of 11 170 emuOe/mol is predicted for $g = 2$ low-spin Co^{II} ($S = 1/2$) antiferromagnetically coupled with Mn^{IV} ($S = 3/2$). Antiferromagnetically coupled high-spin Co^{II} ($S = 3/2$) will lead to zero magnetization. As for Ni^{II}[Mn^{IV}(CN)$_6$], Co^{II}[Mn^{IV}(CN)$_6$] also exhibits frequency dependence in $\chi_{ac}(T)$, indicative of a ferrimagnetic spin-glass-like material. Therefore, the structural disorder in this case leads to both unexpected magnetic ordering at low temperature and spin-glass-like behavior.

Mn^{III}[Mn^{III}(CN)$_6$]. Mn^{III}[Mn^{III}(CN)$_6$] has a room-temperature μ_{eff} of 5.91 μ_B, exceeding the predicted spin-only value of 5.66 μ_B for uncoupled $S = 2$ (high-spin Mn^{III}) and $S = 1$ (low-spin Mn^{III}) spins. The expectation for solely uncoupled high-spin Mn^{III} $S = 2$ spins is 6.93 μ_B, whereas it is 7.07 μ_B for uncoupled $S = 5/2$ (high-spin Mn^{II}) and $S = 3/2$ (Mn^{IV}) spins. This confirms the formulation of Mn^{III}[Mn^{III}(CN)$_6$], consistent with the IR data. The $\mu_{eff}(T)$ decreases with decreasing temperature to a minimum of 5.60 μ_B at 120 K (Figure 3), consistent with the presence of significant first-order spin$-$orbit coupling arising from low-spin [Mn^{III}(CN)$_6$]$^{3-}$ (^{3}T$_1$ ground state)[24] and a second-order spin$-$orbit contribution from the high-spin Mn^{III} ion (^{2}E $\rightarrow$ ^{5}T$_2$).[24] The $1/\chi(T)$ data are not linear because of these contributions; however, extrapolation of the data above 250 K leads to a large θ of -105 K, consistent with the expected antiferromagnetic coupling between high-spin Mn^{III} ($t_{2g}^3e_g^1$) and low-spin [Mn^{III}(CN)$_6$]$^{3-}$ (t_{2g}^4). Below 120 K, $\mu_{eff}(T)$ increases rapidly to a maximum around 26 K.

The low field ZFC magnetization of Mn^{III}[Mn^{III}(CN)$_6$] shows the onset of magnetic order below 31 K (by extrapolation of the steepest slope to M = 0; Figure 4c). Both $\chi'(T)$ and $\chi''(T)$ have two overlapping peaks that are reproducible in their relative positions (Figure 5c). There is no resolvable frequency dependence in the position of the higher temperature peak at T_c, 27 K, but there is frequency dependence in the lower-temperature peak that is clearly resolved in the $\chi''(T)$ data. This lower-temperature, frequency-dependent transition below T_c is characteristic of reentrant spin-glass behavior.[26d,30] The magnetization of 16 840 emuOe/mol at 50 kOe and 5 K (Figure 6) is not

(27) Palacio, F. In *Molecular Assemblies to the Devices: NATO Advanced Studies Workshop*; Coronado, E., Delhaès, P., Gatteschi, D., Miller, J. S., Eds.; Kluwer Academic Publishers: Boston, 1996; Vol. E321, pp 38$-$51.

(28) Zarembowitch, J.; Kahn, O. *New J. Chem.* **1991**, *15*, 181.

(29) Thuéry, P.; Zarembowitch, J. *Inorg. Chem.* **1986**, *25*, 2001.

(30) Brinkerhoff, W. B. Dimensionality and Disorder in Molecule-Based Magnets; Ph. D. dissertation, The Ohio State University, Department of Physics, Columbus, OH, 1995.

saturated. The presence of $\chi''(T)$ is consistent with the observed hysteretic behavior, with a H_{cr} of 8 Oe at 5 K and remanent magnetization of 2000 emuOe/mol (Figure 7c). The initial rise in M(H) lies outside the hysteresis loop and converges with the hysteresis curve above 2 kOe, behavior that is often observed in spin glasses[27] and is seen in the anhydrous $Fe[Mn(CN)_6]$ compound reported.[8] The above data are consistent with $Mn^{III}[Mn^{III}(CN)_6]$ being an ordered ferrimagnet below 27 K and entering a spin-glass state below ca. 20 K.[26d] Such magnetic behavior is not reported for crystalline $Mn^{II}[Mn^{IV}(CN)_6]$ prepared in aqueous media, which has a θ-value of -51.5 K, a room-temperature μ_{eff} of 6.91 μ_B (7.07 μ_B calc.), and a T_c of 48.7 K.[6]

$Cr^{III}[Mn^{III}(CN)_6]$. $Cr^{III}[Mn^{III}(CN)_6]$ has a room-temperature μ_{eff} of 4.62 μ_B, in agreement with, but slightly lower than, the predicted spin-only value of 4.80 μ_B for uncoupled $S = 3/2$ Cr^{III} and $S = 1$ low-spin Mn^{III} spins. The expectation for both uncoupled $S = 3/2$ (Cr^{III} or Mn^{IV}) and $S = 2$ (high-spin Mn^{III} or Cr^{II}) spins is 6.24 μ_B. This is substantially greater than the observed values and confirms the formulation of $Cr^{III}[Mn^{III}(CN)_6]$, consistent with the IR data. The $\mu_{eff}(T)$ decreases with decreasing temperature to a minimum of 3.80 μ_B at 70 K (Figure 3b). This decrease is again attributed to both the first-order spin−orbit coupling from low-spin $[Mn^{III}(CN)_6]^{3-}$ and the presence of strong antiferromagnetic coupling [$\theta = -140$ K ($T > 250$ K)] dominating $\mu_{eff}(T)$. Below 70 K, $\mu_{eff}(T)$ increases rapidly to a maximum around 18 K (Figure 3b), consistent with the low field magnetization curve (Figure 4) that reveals the onset of magnetic order below 22 K.

$\chi'(T)$ for $Cr^{III}[Mn^{III}(CN)_6]$ has one very broad peak, whereas $\chi''(T)$ has two resolved peaks (Figure 5d). The peak in $\chi'(T)$ shows a frequency dependence typical of spin-glass-like materials,[26b] whereas the frequency dependence in $\chi''(T)$ is resolved only in the more intense lower-temperature peak. The 10-Hz $\chi'(T)$ has a peak maximum at 10.6 K that is much lower than the 22 K T_c determined from the M(T) data. In related compounds, T_c determined from $\chi'(T$, 10 Hz) is ~5 K less than the M(T) data extrapolated to M = 0. This trend and the weaker, higher-temperature, frequency-independent $\chi''(T)$ component suggest that there is an overlapping $\chi'(T)$ peak around 16 K. Unfortunately, because of the intensity of the 10.6 K peak, the higher-temperature $\chi'(T)$ peak is not resolved from the broad shoulder. This evidence suggests that $Cr^{III}[Mn^{III}(CN)_6]$ also exhibits reentrant spin-glass behavior like $Mn^{III}[Mn^{III}(CN)_6]$, but the χ-ac peak associated with the glass transition has greater intensity than the peak associated with the ordering transition.

The magnetization at 50 kOe and 5 K is 5050 emuOe/mol (Figure 6), nearly the expected value of 5585 emuOe/mol for antiferromagnetically coupled $S = 3/2$ (Cr^{III}) and low-spin $S = 1$ (Mn^{III}), and is not saturated like the compounds previously described. Hysteresis, consistent with the presence of the $\chi''(T)$, is observed at 5 K ($H_{cr} = 130$ Oe), with a remanent magnetization of 80 emuOe/mol (Figure 7d). The above data are consistent with $Cr^{III}[Mn^{III}(CN)_6]$ being an ordered ferrimagnet below ~16 K and entering a spin-glass state below 10.6 K.

$V^{III}[Mn^{III}(CN)_6]$. $V^{III}[Mn^{III}(CN)_6]$ has a room-temperature μ_{eff} of 3.71 μ_B, which is reduced from predicted spin-only values of 4.00 μ_B for uncoupled $S = 1$ (V^{III} and low-spin Mn^{III}) spins or 5.66 μ_B for uncoupled $S = 1$ (V^{III}) and $S = 2$ (high-spin Mn^{III}) spins. Likewise, this value is less than 5.48 μ_B for uncoupled $S = 3/2$ (V^{II} and Mn^{IV}) spins assuming a formulation of $V^{II}[Mn^{IV}(CN)_6]$. These data are consistent with the formulation derived from IR data of $V^{III}[Mn^{III}(CN)_6]$ and the presence of some $V^{IV}[Mn^{II}(CN)_6]$ (both $S = 1/2$ ions) that will reduce the overall number of spins in the material. The θ-value of -370 K reveals very strong antiferromagnetic coupling dominating the exchange and is significant enough to contribute to a reduction of the room-temperature μ_{eff} from the expected value of 4.00 μ_B. The $\mu_{eff}(T)$ decreases significantly with decreasing temperature down to ca. 40 K then increases rapidly to a maximum around 21 K (Figure 3b). This is consistent with the low field magnetization curve (Figure 4) that reveals the onset of magnetic order below 28 K.

Antiferromagnetic coupling between V^{III} (t_{2g}^2) and low-spin $[Mn^{III}(CN)_6]^{3-}$ (t_{2g}^4) should lead to fully compensated spins and antiferromagnetic ordering at best. (The same is true for V^{IV} (t_{2g}^1) and low-spin $[Mn^{II}(CN)_6]^{4-}$ (t_{2g}^5).) However, the presence of an oxidized vanadyl species or nonstoichiometry of a few percent can lead to a residual magnetization, as is the case for $KV^{II}[Cr^{III}(CN)_6]\cdot 2H_2O$.[5g] The low magnetization value at 50 kOe supports this possibility and is discussed below.

Both $\chi'(T)$ and $\chi''(T)$ of $V^{III}[Mn^{III}(CN)_6]$ are consistent with the presence of magnetic ordering (Figure 5e). The $\chi'(T)$ peak is very broad and may be a combination of two peaks. The 10-Hz peak maximum is at 19 K and is much lower than the ordering temperature approximated from the M(T) data (28 K), as is the case for $Cr^{III}[Mn^{III}(CN)_6]$. Both $\chi'(T)$ and $\chi''(T)$ are frequency-dependent, again typical for spin-glass-like materials.[26b] Two components are not evident in the $\chi''(T)$ data. This may be due to either a higher ordering transition being much weaker in magnitude than a spin-glass transition and/or the onset of these transitions being too close together to resolve. The magnetization at 50 kOe and 5.0 K of 2120 emuOe/mol (Figure 6) is evidence for a significant amount of uncompensated spin at lower temperatures. $V^{III}[Mn^{III}(CN)_6]$, as the presence of the $\chi''(T)$ suggests, exhibits hysteresis with a H_{cr} of 340 Oe at 5 K, and remanent magnetization of 100 emuOe/mol (Figure 7e). The above data are consistent with $V^{III}[Mn^{III}(CN)_6]$ being an ordered ferrimagnetic spin glass below 19 K.

Spin-Glass Behavior. The results above show that each $M[Mn(CN)_6]$ [M = V, Cr, Mn, Fe,[8] Co, Ni] has the necessary component for spin-glass behavior, i.e., spin frustration which is differentiated from geometric frustration. Several examples of strongly geometrically frustrated magnets are known, such as the 2-D triangular magnetic lattices VCl_2 and $NaTiO_2$; cubic 3-D magnets such as the fcc K_2IrCl_6 and zinc blende-structured $MnIn_2Te_4$; and the garnet-structured $Gd_3Ga_5O_{17}$.[26c] The difference between these examples and the Prussian blue lattices is that the magnetic lattices in the examples have nearest-neighbor couplings in a triangular arrangement, whereas the Prussian blue magnetic lattice is cubic. In a Prussian blue lattice there is no spin frustration without a high degree of disorder to create distorted local bonding motifs with differing magnetic exchange coupling parameters. Structural disorder is clearly evident in the X-ray powder diffraction data (Figure 1) and results in the frequency dependence of the ac-χ response.

The normalized frequency shift in the freezing temperature, T_f, of the spin-glass (T at which $\chi'(T)$ is maximum) can be described by the parameter ϕ, eq 1, where T_f is the temperature at which the maximum in $\chi'(T)$ at an initial frequency, ω_i (10 Hz), occurs; ΔT_f is the difference between maxima an initial (10 Hz) and final (ω_f; 1000 Hz) frequencies. The value of ϕ can be used as a criterion to distinguish between different categories of materials exhibiting spin-glass behavior.[26b]

$$\phi = \Delta T_f/[(T_f \Delta(\log \omega))] \quad (1)$$

ϕ is 0.021, 0.033, and 0.052 for $M[Mn(CN)_6]$ (M = V, Cr, Ni), respectively, and is not resolved for M = Mn, Co, because the

frequency-dependent $\chi'(T)$ peak maxima are obscured or at lower temperatures than are experimentally accessible. Frequency dependence in metallic, canonical spin glasses is typically small (e.g., ~0.005 for CuMn alloys), although it is larger in insulating spin-glass-like materials (e.g., 0.06 for (Eu,Sr)S).[26b] The superparamagnet, α-$(Ho_2O_3)(B_2O_3)$, is an extreme case for frequency-dependent behavior, with a value of 0.28.[26b] In this context, $M[Mn(CN)_6]$ (M = V, Cr, Ni) is expected to be a nonconducting spin glass.

Many materials with spin-glass behavior exhibit their glass transition, T_f, at or above T_c. It is less common to see a glass transition below T_c and this behavior is termed "reentrant" because the magnetically ordered state reenters a "disordered" state at lower temperature. This is thermodynamically allowable only when the entropy of the frustrated spin system is reduced by creating cluster domains of spins with local order that are more weakly coupled to neighboring cluster domains in a state of order similar to a true glass.[26] This condition is observed in several of the anisotropic [MnTPP][TCNE] (H_2TPP = *meso*-tetraphenylporphyrin) ferrimagnetic chain compounds.[31] The observation of this state in $M[Mn(CN)_6]$ (M = Cr, Mn) presented here is unexpected, as it is typically thought to be a uniform fcc structure. Due to the structural disorder present in these compounds, it may be reasonable to consider that the stronger (ordered) magnetic exchange pathways give rise to magnetic order at T_c, whereas T_f occurs when the weaker (disordered) exchange pathways contribute to the magnetic order at lower temperature, resulting in the observed reentrant spin-glass behavior.

Hysteretic and Saturation Behavior. Field-dependent M(*H*) data for $M[Mn(CN)_6]$ (M = V, Cr, Mn, Co, Ni) all exhibit hysteretic behavior with coercive fields ranging from 8 (M = Mn) to 340 Oe (M = V) and remanent fields ranging from 4 (M = Co) to 1500 Oe (M = Mn) (Table 5). The hysteretic and saturation behavior of magnetic materials is influenced by several parameters, such as single-ion anisotropy, shape anisotropy, structural defects, disorder, and spin frustration. In disordered materials, such as the ones reported here, there is little chance of deconvoluting the contribution of each parameter, but there are trends that can be considered.

In materials such as the rutile-structured CrO_2 used for magnetic recording media, there is a strong dependence of the coercive field on shape anisotropy (aspect ratio of the particles),[32] whereas the particles in magnetic films of the chromicyanide Prussian blue analogues are symmetric (cubic) and their coercive behavior is strongly influenced by single-ion anisotropy.[5c] Structural disorder tends to decrease the coercive field, whereas impurities can act as domain-wall pinning sites and increase the coercive field. Materials in a frozen spin-glass state have additional random anisotropy axes associated with each of the spin clusters that affect the spin relaxation dynamics and often result in the observation of constricted hysteresis loops (on the relatively short time scale of a typical experiment) and small isothermal remanent magnetizations.[33,34] For example, the external field has to overcome this array of local anisotropy axes to fully align the spin clusters in an equilibrated global energy minimum, which can be relatively slow in a glassy state. The observed response in certain oxides[33] and some canonical spin glasses is that full saturation is not achieved even at 4.2 K and 40 T.[34]

The $M[Mn(CN)_6]$ materials reported here are influenced by many or all of these factors. Single-ion anisotropy associated with the metal centers, structural disorder, and spin-glass behavior are competing effects that determine the strength of the coercive fields. The very low values of the remanent magnetizations (ranging from 0.1 to 12% of the 50 kOe magnetization values) point out that the influence of the spin-glass state is significant. This conclusion is also manifested in the M(*H*) data that does not reach saturation for any of the materials.

The observed low 50 kOe magnetization value for $Ni^{II}[Mn^{IV}(CN)_6]$ (8930 emuOe/mol) relative to the expected ferromagnetic saturation values for $S = 1$ (Ni^{II}) and $S = 3/2$ (Mn^{IV}) of 27925 emuOe/mol (FO coupled) or 5585 emuOe/mol (AF coupled) is consistent with the spin-frustrated nature of a spin-glass material. Because of the presence of competing ferro- and antiferromagnetic interactions rather than just the ferromagnetic coupling that was expected, there will be a reduction in the observed M_s value at the relatively low fields used here.

For $Co^{II}[Mn^{IV}(CN)_6]$, the M(*H*) measurements are made in the vicinity of its ordering temperature, but it still exhibits a small, constricted coercive field due to the onset of magnetic order and spin-glass behavior (Figure 7b). The M(*H*) curve, Figure 6, is more complicated than the typical saturation magnetization curve. At approximately 12 kOe there is a sudden change in slope, and the magnetization increases more rapidly with field again. This is also evident in the hysteresis curve (constricted shape) which traces over the saturation data. The inflection point around 12 kOe is indicative of metamagnetic behavior.[2,26] Metamagnetic behavior is found in materials in which there is a transition between competing antiferro- and ferromagnetic interactions, consistent with the cases here exhibiting spin-glass behavior.

$Mn^{III}[Mn^{III}(CN)_6]$ also exhibits a constricted hysteresis loop (Figure 7c) and an "S"-shaped virgin curve that lies outside the hysteresis loop, due to either the slow relaxation dynamics or possible metamagnetic behavior of the spin-glass state. The *M*(*H*) curve for $Mn^{III}[Mn^{III}(CN)_6]$ does not fully saturate (Figure 6) and the magnetization of 16 840 emuOe/mol lies between the calculated values for ferromagnetically (33 510 emuOe/mol) and antiferromagnetically coupled (11 170 emuOe/mol) $S = 2$ and $S = 1$ ions, again showing that there are mixed ferromagnetic and antiferromagnetic interactions. This behavior is very similar to that of $Fe[Mn(CN)_6]$ prepared under the same conditions.[8]

For $Cr^{III}[Mn^{III}(CN)_6]$, the observed magnetization at 50 kOe is 5050 emuOe/mol (Figure 7d) and is in good agreement with the calculated value of 5585 emuOe/mol for antiferromagnetic coupling between $S = 3/2$ (Cr^{III}) and $S = 1$ (low-spin Mn^{III}). The magnetization does not fully saturate at 50 kOe as a result of being in a spin-glass state.

$V^{III}[Mn^{III}(CN)_6]$ is expected to be fully spin-paired without any residual magnetization. Therefore, the uncompensated spin content leading to bulk magnetic order must be due to the presence of oxidized vanadium or nonstoichiometry, as suggested above and as reported for $KV^{II}[Cr^{III}(CN)_6]\cdot 2H_2O$.[5g] On the basis of the magnetization of 2120 emuOe/mol (compared to 5585 emuOe/mol for one spin), about 38% of V^{III} would have to be oxidized to a $V^{IV}{=}O$ species. However, $\nu_{V=O}$ and

(31) (a) Brandon, E. J.; Rittenberg, D. K.; Arif, A. M.; Miller, J. S. *Inorg. Chem.* **1998**, *37*, 3376. (b) Brandon, E. J.; Arif, A. M.; Burkhart, B. M.; Miller, J. S. *Inorg. Chem.* **1998**, *37*, 2792. (c) Brinckerhoff, W. B.; Morin, B. G.; Brandon, E. J.; Miller, J. S.; Epstein, A. J. *J. Appl. Phys.* **1996**, *79*, 6147.

(32) McCurrie, R. A. *Ferromagnetic Materials*; Academic Press: New York, 1994; Chapter 1.

(33) Ortega, I. J.; Puche, R. S.; de Paz, J. R.; Martínez, J. L. *J. Mater. Chem.* **1999**, *9*, 525.

(34) Mydosh, J. A. *Spin Glasses*; Taylor and Francis: Washington, DC, 1993; pp 88−97.

vanadyl-shifted ν_{CN} absorptions are not observed in the initial IR spectra until after exposure to oxygen. A 19% deficit of either ion could also account for this, but the quantitative yields do not reflect such a significant reduction in mass. Therefore, a combination of these two issues may result in the observed magnetic properties. $V^{III}[Mn^{III}(CN)_6]$ exhibits the largest coercive field of 340 Oe, but the magnetization at 50 kOe is only 2120 emuOe/mol (Figure 7e). This is a likely manifestation of the presence of a detectable amount of $V^{IV}[Mn^{II}(CN)_6]$, some oxidized vanadyl species, or possibly some nonstoichiometry. Each of these "impurities" contributes additional structural inhomogeneities that can inhibit domain-wall movement, relative to the rest of the $M[Mn(CN)_6]$ series.

All of the above materials exhibit complex magnetic behavior as a result of their convoluted structural makeup and are influenced by subtle changes in the synthetic parameters used to synthesize and isolate them. The results are qualitatively reproducible and consistent, but there is always some variation from one preparation to the next with respect to crystallinity, particle size, and occluded byproduct. For M = V, the V center was very sensitive to oxidation by oxygen, as with other V-containing Prussian blue analogues,[5d−g] thus contributing additional complications to consistent magnetic characterization.

Conclusion

The $M^{II}[Mn^{IV}(CN)_6]$ (M = Co, Ni) and $M^{III}[Mn^{III}(CN)_6]$ (M = V, Cr, Mn) Prussian blue analogues made in nonaqueous media were characterized by several techniques and found to be consistent with the proposed formulations. The structures are consistent with the fcc Prussian blue lattice, but they suffer severely from structural disorder. The room-temperature μ_{eff} values are consistent with the formulations showing significant contributions from structural disorder, particularly for M = Co. All of these compounds exhibit spontaneous magnetic ordering at low temperatures and the onset of spin-glass behavior very close to or below their magnetic ordering temperatures.

Prussian blue lattices are normally formed with zeolitic water and/or charge-balancing cations (i.e., K^+, Cs^+) filling the open pore space within the structure and are structurally analyzed as microcrystalline powders and single crystals. However, because of the extreme hydrolytic instability of the $[Mn^{IV}(CN)_6]^{2-}$, all of the syntheses and measurements of the physical properties were performed under rigorously anhydrous conditions. The absence of water during lattice formation has a profound effect on the crystallinity and magnetic properties of these anhydrous Prussian blue analogues. Rather than behaving as ferro- (M = Ni), ferri- (M = Cr, Mn), and antiferro- (M = V, Co) magnets with well-defined magnetic exchange parameters, these materials offer an opportunity to study the experimental effects of inhomogeneous exchange parameters and spin-glass behavior in a 3-D mixed-valent bimetallic system. Spin-glass behavior is the most prominent behavior observed, one that is not expected in Prussian blue materials.

This study has shown that a strong relationship exists between structure, disorder, and magnetic behavior in the Prussian blue analogues. These nonaqueous analogues are significantly disordered, exhibiting many deviations from the expected magnetic behavior, and possess properties normally associated with highly disordered/spin-frustrated materials. Further investigations into these nonaqueous Prussian blue analogues and related systems should continue to reveal new behavior not observed in the aqueous compounds.

Acknowledgment. The authors gratefully acknowledge the U. S. Department of Energy (Grant No. DE-FG03-93ER45504) for support of this work and helpful discussions with Jamie L. Manson.

IC991308Y